AIAA JOURNAL
Vol. 35, No. 6, June 1997

Linear Stability of Hypersonic Flow in Thermochemical Nonequilibrium

Mary L. Hudson* and Ndaona Chokani†
North Carolina State University, Raleigh, North Carolina 27695-7910
and
Graham V. Candler‡
University of Minnesota, Minneapolis, Minnesota 55455

For flight at high Mach numbers, thermal and chemical nonequilibrium may exist in the mean flow and thus affect the stability of the flow. A computational tool was developed to analyze a hypersonic mean flow and its stability including thermochemical nonequilibrium. The mean flow analysis employs the Navier–Stokes equations with a translational/vibrational temperature model for thermal nonequilibrium and a five-species reacting air model for chemical nonequilibrium. The stability analysis employs linear stability theory to describe the spatial amplification of two- and three-dimensional disturbances. The computational tool is used to determine the frequency and spatial amplification of disturbances that may lead to boundary layer transition on cold wall and adiabatic flat plates. The effect of thermal and chemical nonequilibrium on stability is shown to depend on the disturbance mode.

I. Introduction

THE transition from laminar to turbulent flow significantly affects the surface heating as well as the aerodynamic performance of a hypersonic vehicle. Thus, an accurate prediction of boundary-layer transition is necessary for an optimum design of the vehicle and its thermal protection system. Historically, empirical relationships, based on re-entry vehicle flight data, were developed to predict the location of transition. An accurate prediction of transition on a re-entry vehicle was not so critical, because the ablating thermal protection system was conservatively designed to survive a one-time use mission. However, for new vehicles, such as reusable hypersonic cruise vehicles and aerobrakes for Earth and Mars entry missions, weight limitations dictate mission feasibility and therefore reduce the allowable degree of design conservatism. Thus, a more accurate simulation of boundary-layer transition is necessary to design new hypersonic vehicles.

In stability analyses, the fundamental causes of boundary-layer transition are identified. In this approach, the frequency and amplification rates of disturbances in a specified mean flow are examined. The predicted stability of these disturbances depends on the character of the mean flow. In a hypersonic flow, the gas can be vibrationally excited and may dissociate and recombine; thermal and chemical nonequilibrium may thus affect the stability of the flow. To date, most stability analyses of hypersonic flows have assumed perfect gas. Two exceptions to this are the works led by Malik[1,2] and Stuckert.[3,4] Malik and Anderson[1] employed the boundary-layer equations to examine equilibrium airflow over a flat plate. Stuckert and Reed[3] solved the parabolized Navier–Stokes equations to study the chemical nonequilibrium flow over an axisymmetric cone. The objective of the present work is to examine the effects of thermochemical nonequilibrium on the linear stability of a hypersonic flow. The approach undertaken in the work is to first solve the full Navier–Stokes equations with a two-temperature model and five-species air model. Then, the stability of the spatially evolving disturbances is examined from the linearized disturbance equations.

There are two modes of inviscid instability for hypersonic flow. The first mode is a vorticity disturbance, and the second mode is an acoustic disturbance. The two modes can be described by defining a local Mach number, $\bar{M}$, relative to the phase velocity c_r

$$\bar{M} = (u - c_r)/a$$

where u is the local velocity parallel to the surface and a is the local speed of sound.

If $\bar{M}^2 < 1$ everywhere, Lees and Lin[5] showed that the presence of a generalized inflection point (gip), defined as

$$\frac{\partial}{\partial y}\left(\rho\frac{\partial u}{\partial y}\right) = 0$$

which indicates a maximum in the angular momentum, is a sufficient condition for first-mode instability. For compressible perfect gas flow, the most unstable first-mode disturbance is always oblique, and there is a unique wave number corresponding to the phase velocity at the gip. In our previous work,[6] we qualitatively assessed thermochemical nonequilibrium effects on first-mode instability by examining the location of the gip in the mean flow around a sphere. In the present work, the linear stability analysis is used to quantify these effects.

The higher frequency second-mode disturbance has been shown to be the most unstable in perfect gas hypersonic flows. If $\bar{M}^2 > 1$, then the boundary layer is unstable to inviscid waves regardless of any other feature of the profile. Unlike the first mode, there is a multiplicity of unstable modes.[7,8] For the second and higher modes, two-dimensional disturbances are the most unstable. Whereas in our previous work the analysis was limited to first-mode disturbances, the present work extends the analysis to include the second-mode disturbances.

In this paper, we present the development of a computational tool to evaluate the first- and second-mode disturbances in a hypersonic mean flow with thermal and chemical nonequilibrium. In Secs. II and III, the governing equations and numerical methods for the mean flow and disturbances with thermochemical nonequilibrium are presented. The validation of the numerical methods is presented in Sec. IV; the results are compared with previous results of perfect gas, equilibrium air, and chemical nonequilibrium air models. The effects of thermal and chemical nonequilibrium are then examined in Sec. V.

Presented as Paper 96-0671 at the AIAA 34th Aerospace Sciences Meeting and Exhibit, Reno, NV, Jan. 15–18, 1996; received June 14, 1996; revision received March 13, 1997; accepted for publication March 16, 1997.

*Graduate Research Assistant, Department of Mechanical and Aerospace Engineering; currently Senior Member, Technical Staff, Sandia National Laboratories, Albuquerque, NM 87185-0827. Senior Member AIAA.

†Associate Professor, Department of Mechanical and Aerospace Engineering. Senior Member AIAA.

‡Associate Professor, Department of Aerospace Engineering and Mechanics. Senior Member AIAA.

II. Mean Flow

A. Governing Equations

The Navier–Stokes equations are employed to describe the flow of nonequilibrium air over a body. The analysis employs a two-temperature model for thermal nonequilibrium and five-species air model for chemical nonequilibrium. Thus, five-species equations, two momentum equations, and two energy equations are solved. The governing mean flow equations in conservative form and Cartesian coordinates are as follows:

$$\frac{\partial U}{\partial t} + \frac{\partial F}{\partial x} + \frac{\partial G}{\partial y} = W \tag{1}$$

where the vector of conserved variables is

$$U = \{\rho_1, \rho_2, \rho_3, \rho_4, \rho_5, \rho u, \rho v, E_{\text{vib}}, E_{\text{total}}\}^T$$

$\rho_s, s = 1, 5$, are the species mass densities, u and v are the tangential and body-normal velocities, and E_{vib} and E_{total} are the vibrational and total energy; t, x, and y are the time, streamwise direction, and body-normal direction, respectively. F and G are the flux vectors and W is the source vector, which has terms in the species and vibrational energy equations, as detailed in Refs. 9 and 10.

The following three dissociation reactions and two exchange reactions in air are modeled, where M is any collision partner (such as N_2, O_2, NO, N, or O):

$$N_2 + M \leftrightarrow 2N + M$$

$$O_2 + M \leftrightarrow 2O + M$$

$$NO + M \leftrightarrow N + O + M$$

$$N_2 + O \leftrightarrow NO + N$$

$$NO + O \leftrightarrow O_2 + N$$

The equilibrium constants, transport properties, and translational–vibrational energy exchange source term are modeled following Candler and MacCormack.[10] The boundary conditions at the wall are no-slip, noncatalytic, and either constant temperature or adiabatic.

The same equations and reactions are used to separately model equilibrium, chemical nonequilibrium, and thermochemical nonequilibrium air. This was accomplished by adjusting the vibrational relaxation times and chemical reaction rates. For thermal equilibrium, the vibrational relaxation times were decreased by a factor of 10^4. For chemical equilibrium, the forward and backward reaction rates were increased by a factor of up to 10^6. This technique worked very well to simulate the various reacting flows. The equivalence of the translational and vibrational temperatures confirmed thermal equilibrium. Chemical equilibrium was attained when there was negligible difference in the mass concentration ratios as the reaction rates were increased.

B. Numerical Method

A modified Steger–Warming flux vector splitting upwind numerical technique, presented by MacCormack and Candler,[11] is used to solve the Navier–Stokes equations. This technique is fully implicit and uses the Gauss–Seidel line relaxation procedure. The highly vectorized code of these equations and numerical method was employed in our previous work.[6]

In anticipation of the stability analysis, the grid for the mean flow computations was generated with body-normal grid lines normal to the surface. Stability calculations also require the grid to capture physical aspects of the flow, which indicate stability behavior. So a grid-point distribution was formulated so that points were clustered in the vicinity of the generalized inflection point and the shock.

III. Linear Stability Analysis

A. Governing Equations

The stability equations of the disturbances in a thermochemical nonequilibrium hypersonic flow are derived from the Navier–Stokes equations [Eq. (1)]. The instantaneous flow is first modeled by a mean plus fluctuating component, $q = \bar{q} + q'$. The equations are then linearized with respect to the fluctuations, and the mean flow is subtracted. The mean flow is assumed parallel so that $\bar{q}(x, y, z) = \bar{q}(y)$, where x, y, and z are in the streamwise, surface normal, and azimuthal directions, respectively. The resulting linearized perturbation equations for thermochemical nonequilibrium flow are detailed in Ref. 9. The stability equations are then obtained by assuming that the fluctuations are given by a normal mode

$$q'(x, y, z, t) = \hat{q}(y) \exp[i(\alpha x + \beta z - \omega t)]$$

where $\hat{q}$ = complex amplitude of the disturbance, $\alpha = \alpha_r + i\alpha_i$ = streamwise wave number, β = azimuthal wave number, and ω = disturbance frequency.

The relevant spatial evolution of the hypersonic flow is considered in the present formulation, so that the frequency is real and the wave numbers are complex. The disturbances are then unstable if the streamwise spatial amplification rate $-\alpha_i > 0$. Substituting the normal mode into the linearized equations, a system of 10 ordinary differential equations is obtained for thermochemical nonequilibrium:

$$\left(A\frac{\mathrm{d}^2}{\mathrm{d}y^2} + B\frac{\mathrm{d}}{\mathrm{d}y} + C \right) \boldsymbol{Z} = 0 \tag{2}$$

where $\boldsymbol{Z} = (\hat{\rho}_s, \hat{u}, \hat{v}, \hat{w}, \hat{T}, \hat{T}_v)$; $s = 1$ to 5 species; $\hat{u}$, $\hat{v}$, and $\hat{w}$ are the disturbance velocities in the x, y, and z directions, respectively; and $\hat{T}$ and $\hat{T}_v$ are the amplitudes of the translational and vibrational temperatures, respectively. A is a diagonal matrix and B and C are 10×10 complex matrices. These matrices are a function of the mean flow, α, β, and ω and are presented by Hudson.[9]

The stability boundary conditions are applied as follows. At the wall, the velocity and temperature disturbances are zero. In addition, a noncatalytic wall is assumed so that a zero normal gradient of the species mass concentration is specified. In the freestream, all disturbances except the body-normal disturbance velocity are assumed zero. A numerical boundary condition is required at the freestream boundary to avoid a trivial solution. So, following the work of Stuckert,[4] the mixture mass conservation equation is used to obtain the body-normal velocity.

In the present work, the freestream properties and a reference length, defined as

$$l_{\text{ref}} = \sqrt{\nu_\infty x / u_\infty} = x/\sqrt{Re_x} = x/R$$

are used to nondimensionalize the wavelength and frequency.

B. Numerical Method

Because nonzero solutions that satisfy the boundary conditions exist only for certain combinations of the wave numbers and frequency, Eq. (2) constitutes an eigenvalue problem. For spatial stability, the eigenvalue to be determined is the complex streamwise wave number α for a specified real frequency ω and real spanwise wave number β:

$$\alpha = \Omega(\omega, \beta) \tag{3}$$

The eigenvalue problem can be solved by either a global or a local method. Following the work of Malik,[12] the global method, which yields a spectrum of approximate eigenvalues, is used to provide an initial estimate for the local method. The approximate eigenvalues from the global method are then improved by the local scheme. The stability analysis was conducted on a uniform computational grid.

C. Global Method

Second-order accurate central differences are used in the global method to approximate the first and second derivatives in the system of ordinary differential equations [Eq. (2)]. The resulting block (10×10) tridiagonal matrix is given by

$$\hat{B}\boldsymbol{Z}_{j+1} + \hat{A}\boldsymbol{Z}_j + \hat{C}\boldsymbol{Z}_{j-1} = 0 \qquad \text{or} \qquad \bar{A}\boldsymbol{Z} = 0 \tag{4}$$

where

$$\hat{B} = \left(\frac{\eta_y^2}{\Delta\eta^2} + \frac{\eta_{yy}}{2\Delta\eta} \right) A + \frac{\eta_y}{2\Delta\eta} B$$

$$\hat{A} = \frac{-2\eta_y^2}{\Delta\eta^2} A + C$$

$$\hat{C} = \left(\frac{\eta_y^2}{\Delta\eta^2} - \frac{\eta_{yy}}{2\Delta\eta} \right) A - \frac{\eta_y}{2\Delta\eta} B$$

η is the body normal coordinate, and subscript j is an index in the η direction.

To solve for the complex streamwise wave number α, Eq. (4) is written as a generalized complex eigenvalue problem

$$\tilde{A}Z = \alpha \tilde{B} Z \tag{5}$$

where $(\tilde{A} - \alpha\tilde{B}) = \bar{A}$ and we assume $\alpha^2 = 0$ following Khorrami and Malik.[13] The wall and freestream boundary conditions are included[9] to reduce the size of the square complex matrices $\tilde{A}$ and $\tilde{B}$ from $10 \times J$ to $10 \times (J - 2)$, where J is the number of stability grid points. The QZ algorithm[14] was used to solve the generalized complex eigenvalue problem.

The global method yields a spectrum of $10 \times (J - 2)$ eigenvalues, α, and their associated eigenvectors Z. A series of filter criteria were developed to select the "desired" eigenvalue from the spectrum. The desired eigenvalue with respect to stability analysis is the most unstable physical one, i.e., $\alpha_r > 0$ and $-\alpha_i > 0$. The three filter criteria were as follows. First, the relative Mach number $\bar{M}$ at the boundary-layer edge is used to select the subsonic unstable eigenvalues. Second, the unstable eigenvalues with positive relative Mach numbers, that is, the phase velocity is less than the local velocity at the edge of the boundary layer, are selected. Finally, the unstable eigenvalues with a phase velocity between 90 and 100% of the freestream velocity are selected. If more than one eigenvalue from the spectrum satisfied these three criteria, each unstable physical eigenvalue was refined by the local method, and the one found to be most unstable was selected.

D. Local Method

The approximate eigenvalue from the second-order global method was then improved upon using the higher-order local method. In the local method, the α^2 terms in Eq. (2) are included. The local method employed a fourth-order accurate finite-difference scheme[15] to approximate the first and second derivatives in Eq. (2). Second-order approximations are used at the boundaries. The resulting 10×10 block pentadiagonal matrix is given by

$$\hat{D}Z_{j+2} + \hat{B}Z_{j+1} + \hat{A}Z_j + \hat{C}Z_{j-1} + \hat{E}Z_{j-2} = 0$$

$$\text{or} \qquad \bar{A}Z = 0 \tag{6}$$

where

$$\hat{D} = -\left(\frac{\eta_y^2}{12\Delta\eta^2} + \frac{\eta_{yy}}{12\Delta\eta} \right) A - \frac{\eta_y}{12\Delta\eta} B$$

$$\hat{B} = \left(\frac{4\eta_y^2}{3\Delta\eta^2} + \frac{2\eta_{yy}}{3\Delta\eta} \right) A + \frac{2\eta_y}{3\Delta\eta} B$$

$$\hat{A} = \frac{-5\eta_y^2}{2\Delta\eta^2} A + C$$

$$\hat{C} = \left(\frac{4\eta_y^2}{3\Delta\eta^2} - \frac{2\eta_{yy}}{3\Delta\eta} \right) A - \frac{2\eta_y}{3\Delta\eta} B$$

$$\hat{E} = \left(\frac{-\eta_y^2}{12\Delta\eta^2} + \frac{\eta_{yy}}{12\Delta\eta} \right) A + \frac{\eta_y}{12\Delta\eta} B$$

Because Eq. (6) is homogeneous, nonhomogeneous boundary conditions are imposed at the wall to avoid a trivial solution. The boundary condition for the velocity perturbation at the wall, $\hat{u}(0) = 0$, is thus replaced by

$$\sum_{s}^{5} \hat{\rho}_s(0)/\rho_\infty = 1$$

which normalizes the eigenvectors by the disturbance mixture density at the wall. With this boundary condition, Eq. (6) becomes $\bar{A}Z = \bar{B}$. LU decomposition was used to solve for Z given an initial estimate of α from the global method. Subsequent values of α were obtained by using a secant iteration on the boundary condition $\hat{u}(0) = 0$. Typically, five iterations were required to obtain a converged solution of $\hat{u}(0)$ to within some tolerance of zero. To compute the eigenvalues for several frequencies, the improved eigenvalue from the local method was extrapolated to provide the guess for the next frequency. This technique was found to be much more efficient than performing a global computation for each frequency.

IV. Code Validation

The thermochemical nonequilibrium stability code was validated by comparing the present computations with results in the literature for perfect gas, equilibrium air, and chemical nonequilibrium air. The accuracy of the global and local methods was first assessed for a perfect gas model. Note that the codes to compute the mean flow and stability of perfect gas are separate from those for thermochemical nonequilibrium and directly follow the work of Malik.[12] The validated numerical methods for the perfect gas model were then applied to the reacting air models. The conditions examined in the stability code validation study included subsonic to hypersonic flows; adiabatic and cold wall surfaces; two- and three-dimensional disturbances; and perfect gas, equilibrium air, and chemical nonequilibrium air models. Full details of the validation study are presented in Ref. 9. Some salient features of the validations are presented here.

A. Perfect Gas

The Mach 10 perfect gas flow over an adiabatic wall flat plate was computed and compared with a self-similar solution and with Ref. 2. The freestream temperature was 277.8 K, unit Reynolds number was 9.8425×10^6/m, and Prandtl number was 0.70. The spatial amplification rates of the Navier–Stokes mean flow solutions on five grids are shown in Table 1. Three of the grids, 150×200, 220×300, and 220×300C, had a conventional wall-clustered distribution, where the grid spacing was minimum adjacent to the wall and maximum at the outer boundary. In the grids designated B and D, the minimum grid spacings were at the shock and near the generalized inflection point; the maximum spacing was in the region between the boundary-layer edge and the shock. The last column in the table shows the percentage error in $-\alpha_i$ compared with the self-similar solution. As the grid is refined near the boundary-layer edge, the predicted amplification rate approaches that of the self-similar solution. The grid with the highest density of points in the vicinity of the generalized inflection point yields the best results; the peak in the angular momentum must be adequately captured to obtain accurate stability results.

B. Equilibrium

The stability of a Mach 10 equilibrium airflow over an adiabatic wall flat plate was next examined. In the present work, the equilibrium airflow was simulated by adjusting the chemical reaction rates and thermal relaxation times as previously described. The suitability of this approach was evaluated by comparing our predictions with

Table 1 Mean flow grid effect on amplification rates; perfect gas, $\omega = 0.08$, $x = 0.4$ m

Grid	(α_r, α_i)	Error, %
Self-similar	(0.0842, $-1.361e{-3}$)	0
Malik[2]	(?, $-1.35e{-3}$)	0.08
150×200	(0.0860, $+3.399e{-5}$)	(stable)
220×300	(0.0857, $-1.261e{-4}$)	90.7
220×300C	(0.0853, $-7.107e{-4}$)	47.8
220×300D	(0.0845, $-1.223e{-3}$)	10.1
270×300B	(0.0843, $-1.379e{-3}$)	1.3

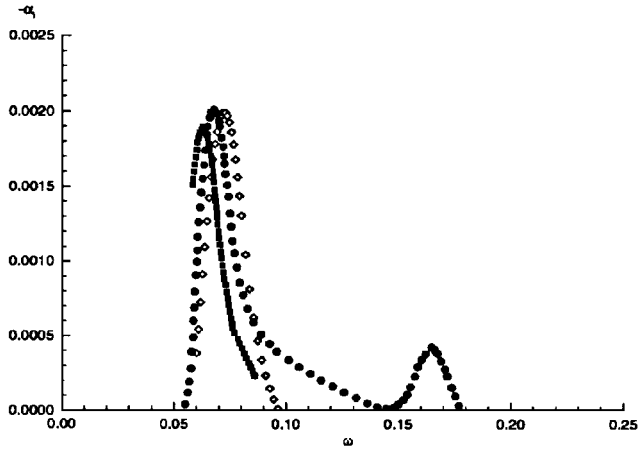

Fig. 1 Amplification rates of second-mode disturbances (Mach 10, equilibrium air, adiabatic wall, and $x = 0.4$ m): ◇ present study; ● Malik[2]; and ■, Stuckert and Reed.[3]

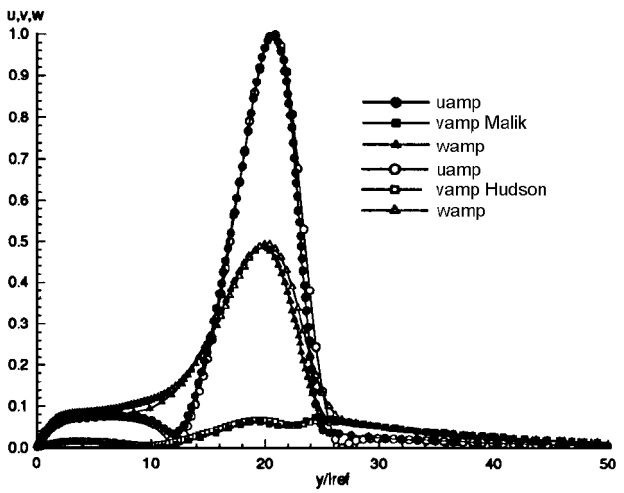

Fig. 2 Amplitude of velocities of first-mode disturbances (Mach 10, equilibrium air, adiabatic wall, $x = 0.4$ m, $\omega = 0.03$, and $\psi = 63$ deg).

the stability results of Malik[2] and of Stuckert and Reed.[3] This validation study also served to examine the effects of the different governing equations, chemical kinetics, and the thermodynamic and transport properties used by each researcher on the stability of the flow.

The spatial amplification rates of two-dimensional disturbances in the equilibrium airflow at $x = 0.4$ m are shown in Fig. 1. In spite of the differences in the equilibrium air models, the predicted peak amplification rates and their associated frequencies are all quite similar. There was also good agreement with the eigenfunction profiles of the most amplified second-mode, which were computed by Malik and Anderson.[1]

As a further validation, the most unstable oblique first-mode disturbance was examined. The amplitudes of all three velocity components compare very well with Malik and Anderson,[1] as shown in Fig. 2. The overall good agreement of both the spatial amplification rates and the eigenfunction profiles for both the first- and second-mode instabilities validates our modeling approach in a reacting gas flow.

C. Chemical Nonequilibrium

The final validation test case was the Mach 10 flow of air in chemical nonequilibrium over an adiabatic wall flat plate. The vibrational relaxation times were adjusted in our thermochemical nonequilibrium flow code to model thermal equilibrium. The stability of the flow is compared with the results of Stuckert and Reed[3] in Fig. 3. The qualitative agreement between the two predictions is good. Quantitatively, our maximum amplification rate is 19% higher at a frequency that is 7.5% higher than that of Stuckert and Reed. For equilibrium air, we computed a similar trend with a 4.5% higher amplification rate at a 13% higher frequency (Fig. 1). The discrepancies in the

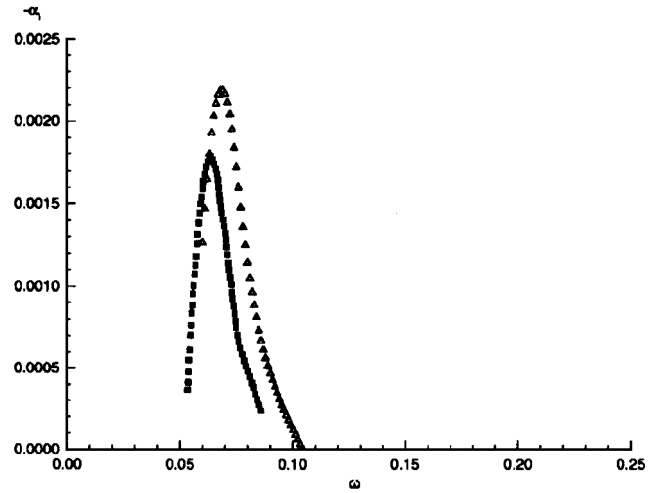

Fig. 3 Amplification rates of second-mode disturbances (Mach 10, chemical nonequilibrium air, adiabatic wall, and $x = 0.4$ m): △, present study; and ■, Stuckert and Reed.[3]

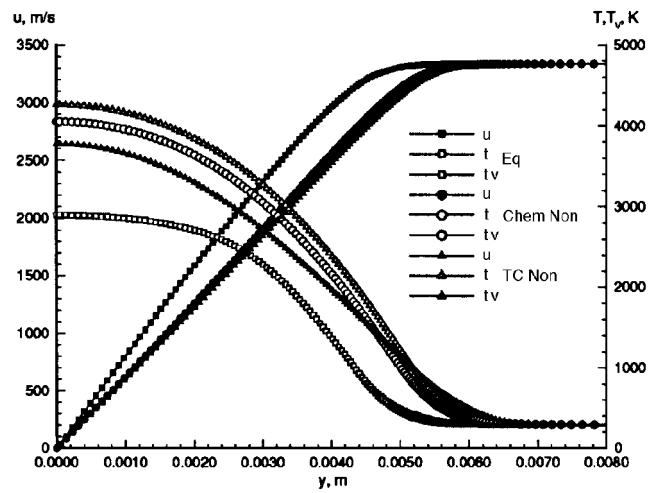

Fig. 4 Mean velocity and temperature profiles (Mach 10, adiabatic wall, and $x = 0.4$ m).

amplification rates are probably due to the differences between the governing equations, property models, and numerical techniques in both the mean flow and stability analyses.

V. Results and Discussion

The validated stability code was used to assess the effects of thermochemical nonequilibrium on the stability of three reacting hypersonic flows: Mach 10 over an adiabatic plate, Mach 10 over a cold wall plate, and Mach 15 over a cold wall plate. For each case, the three gas models—equilibrium air, chemical nonequilibrium air, and thermochemical nonequilibrium air—were simulated. The stability characteristics of first-mode and second-mode disturbances were examined for each flow. In addition, these stability characteristics are used to clarify the observations in two recent high-enthalpy hypersonic transition flow experiments.

A. Case 1: Mach 10, Adiabatic Wall Flat Plate

The freestream conditions for the flow over a 0.5-m-long adiabatic flat plate were a Mach number of 10, freestream temperature of 278 K, and unit Re of 9.8425×10^6/m. The effects of the three gas models on the mean flow velocity and temperature profiles are shown in Fig. 4 at location $x = 0.4$ m. The difference between the translational and vibrational temperatures indicates thermal nonequilibrium, whereas the equivalence of these temperatures verifies our technique for modeling thermal equilibrium. The highest translational temperatures occur with the thermochemical nonequilibrium air model because of the vibration–dissociation coupling, whereby the energy absorption by dissociation is limited because of the slow reaction rates.

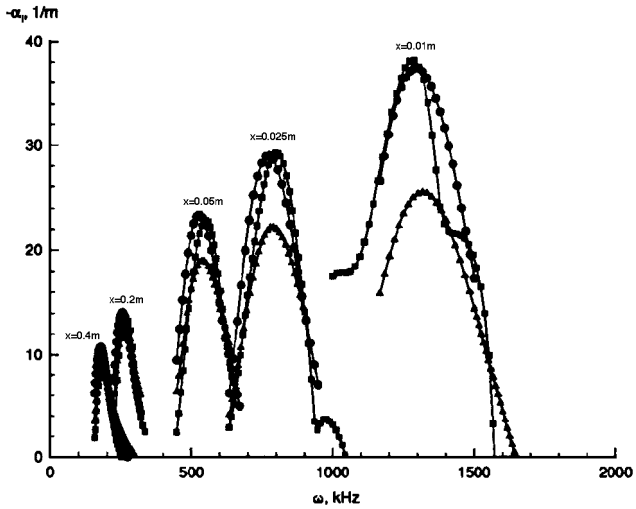

Fig. 5 Amplification rates of second-mode disturbances (Mach 10 and adiabatic wall): ■, Eq; ●, Chem non; and ▲, TC non.

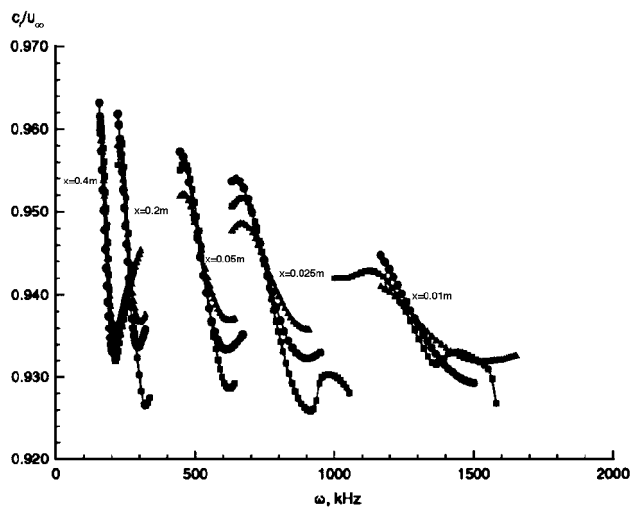

Fig. 6 Phase velocities of second-mode disturbances (Mach 10 and adiabatic wall): ■, Eq; ●, Chem non; and ▲, TC non.

The flow becomes more equilibrium-like in the downstream direction because of the increased flow residence time. Thus, we can anticipate that the flow stability will become more similar for the three gas models at downstream locations. The adiabatic wall temperatures also vary in the axial direction and with the air model. The thermochemical nonequilibrium model has the most elevated wall temperature, 4300 K at $x = 0.4$ m, and the equilibrium air model has the least elevated temperature, 2950 K. The stability of the flow over an adiabatic surface is thus affected by both the nonequilibrium and the varying wall temperatures.

The dimensional amplification rates of the two-dimensional disturbances are shown as a function of the dimensional frequency in Fig. 5 at five axial locations. For all gas models, the maximum spatial amplification rate decreases with increasing x. At the two upstream locations, the equilibrium air model yields the most unstable disturbances; farther downstream, the chemical nonequilibrium air model gives the most unstable disturbances. At all locations, the thermochemical nonequilibrium model gives the least unstable disturbances, which indicates that thermal nonequilibrium and the higher wall temperature have a stabilizing effect on the flow.

Similar to a perfect gas flow, the boundary layer is "tuned" to select frequencies. The frequency of the most-amplified second-mode disturbance decreases from about 1.3 MHz to 190 kHz from the leading edge of the plate downstream, as shown in Fig. 5. At a given axial location, the thermochemical nonequilibrium air model with a thicker boundary layer has a higher most-amplified frequency than the equilibrium and chemical nonequilibrium gas models, which have thinner boundary layers. Figure 6 shows the phase velocities

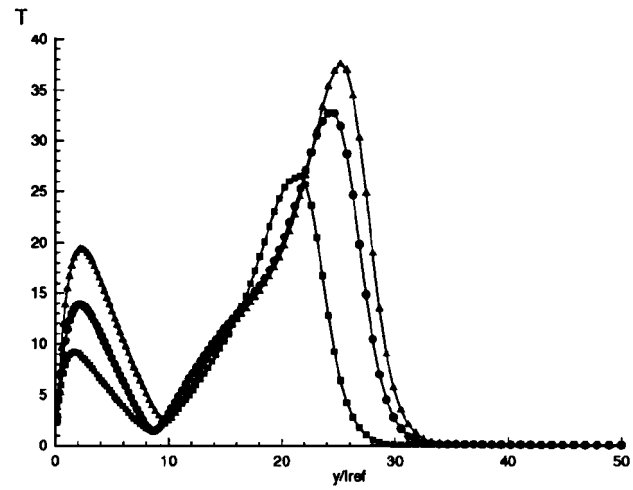

Fig. 7 Amplitude of temperature of second-mode disturbances (Mach 10, adiabatic wall, and $x = 0.4$ m): ■, Eq; ●, Chem non; and ▲, TC non.

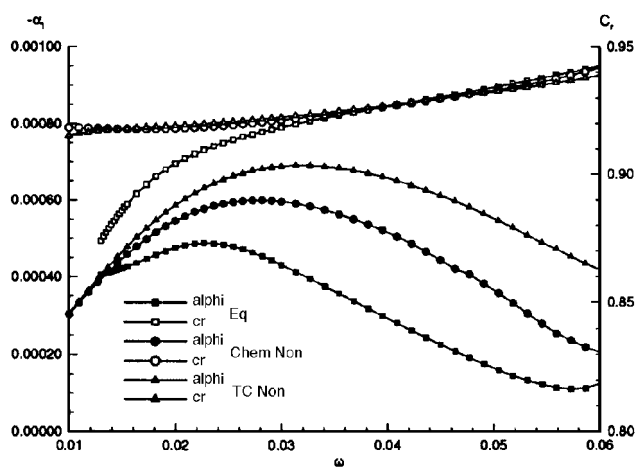

Fig. 8 Amplification and phase velocity of first-mode disturbances (Mach 10, adiabatic wall, $x = 0.4$ m, and $\beta_r = 0.0628$).

at the five axial locations. The phase velocities vary between 93 and 96% of the freestream velocity, and the maximum spatial amplification rates occur at 94% of the freestream velocity.

The details of the mode structure of the most-amplified second-mode disturbance at $x = 0.4$ m are indicated by the amplitude of the temperature eigenfunction in Fig. 7. Qualitatively, there is little difference in the mode structure between the three gas models. The largest amplitudes occur with the thermochemical nonequilibrium air model, and the smallest amplitudes occur with the equilibrium air model. A pressure phase change across the boundary layers of 140 deg confirms the second-mode character of the disturbances.

A first-mode disturbance was analyzed for various frequencies at $x = 0.4$ m and $\beta_r = 0.0628$. The spatial amplification rates and phase velocities are shown in Fig. 8. The flow is the most unstable with thermochemical nonequilibrium and the least unstable with equilibrium. This behavior is exactly as predicted from the angular momentum profiles and wall temperatures; for the flow in thermochemical nonequilibrium, the peak in angular momentum is located the furthest from the wall and the wall temperature is the highest. For first-mode disturbances at these wave angles, the spatial amplification is three to four times less than the second-mode amplification. Also, the maximum amplified frequencies of 60–82 kHz are two to three times less than those of the second-mode disturbances.

B. Case 2: Mach 10, Cold Wall Flat Plate

The effects of wall cooling on the stability of reacting flows were next examined. The same freestream conditions as case 1 were examined for the flow over a constant wall temperature (1200 K) flat plate. The mean velocity and temperature profiles are shown in Fig. 9 at the location $x = 0.4$ m for all three gas models. For these

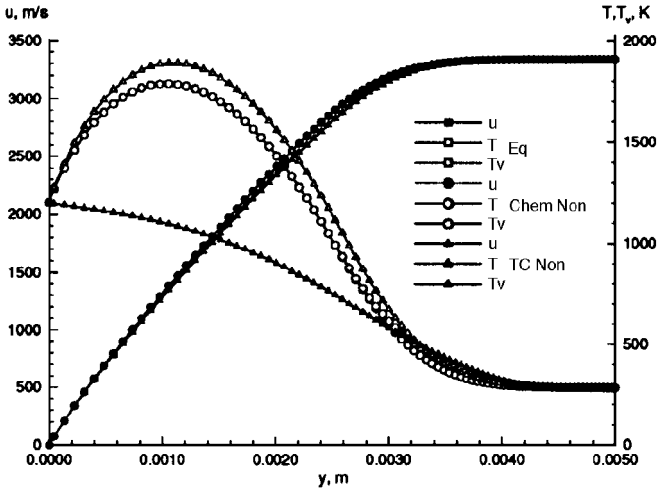

Fig. 9 Mean velocity and temperature profiles (Mach 10, cold wall, and $x = 0.4$ m).

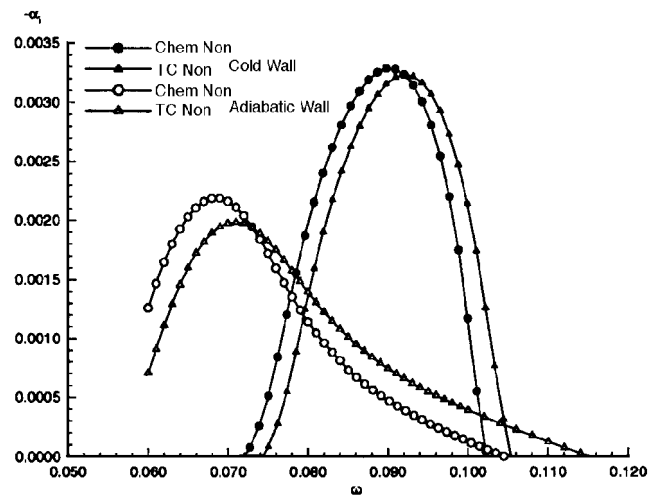

Fig. 10 Amplification rates of second-mode disturbances (Mach 10, adiabatic and cold wall, and $x = 0.4$ m).

flow conditions, the equilibrium and chemical nonequilibrium gas models yielded identical profiles, and the thermochemical nonequilibrium gas model yielded profiles only slightly different from the other two models. The stability of these flows is thus expected to be dominated by the effects of wall cooling.

The spatial amplification rates with the chemical nonequilibrium and thermochemical nonequilibrium gas models on both the adiabatic and cold wall plates are shown in Fig. 10. Wall cooling has a destabilizing effect on the second-mode disturbances. The maximum amplification of the second-mode disturbance on the cold plate is 1.5 times greater than that on the adiabatic plate. In addition, the frequency corresponding to the most-amplified disturbance is shifted to a higher value. This change in the stability behavior clarifies the observations of He and Morgan[16] in their high-enthalpy shock tunnel experiments. They observed that the transition Reynolds number decreased with wall cooling. The present stability results, which describe the precursor to transition, verify that their observations are a consequence of more unstable second-mode disturbances in both chemical and thermochemical nonequilibrium flows.

C. Case 3: Mach 15, Cold Wall Flat Plate

The third case examined was the Mach 15 flow past a cold wall (1225 K) flat plate. The freestream temperature and unit Reynolds number were 700 K and 3.4×10^6/m, respectively. The mean flow velocity and temperature profiles at $x = 0.294$ m are shown in Fig. 11 and the oxygen mass concentration profiles through the boundary layer are shown in Fig. 12. It is evident that there are differing degrees of chemical reaction between the three gas models. The thermochemical nonequilibrium air model has the least degree

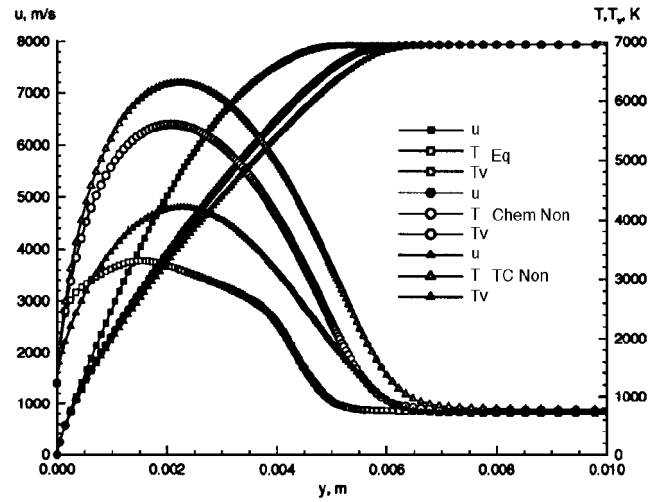

Fig. 11 Mean velocity and temperature profiles (Mach 15, cold wall, and $x = 0.294$ m).

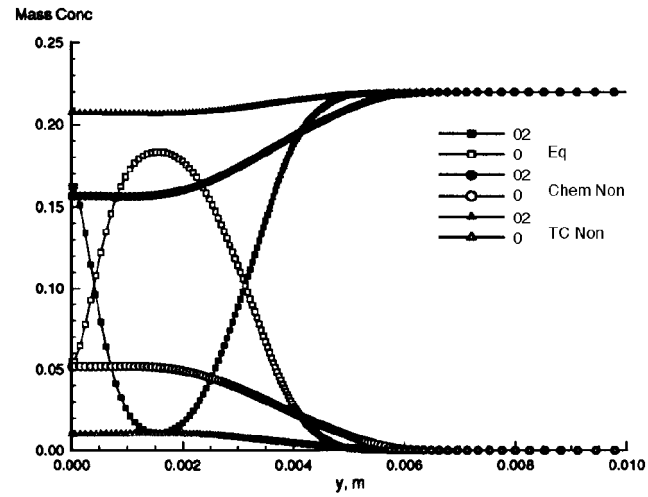

Fig. 12 Oxygen mass concentration profiles (Mach 15, cold wall, and $x = 0.294$ m).

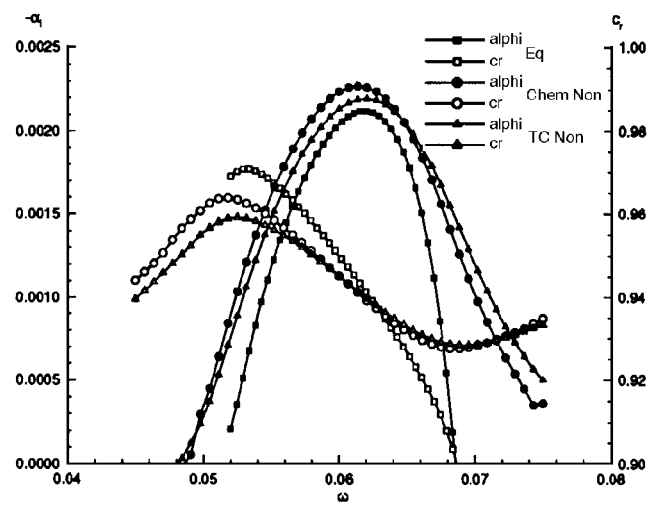

Fig. 13 Amplification and phase velocity of second-mode disturbances (Mach 15, cold wall, and $x = 0.294$ m).

of oxygen dissociation, and the equilibrium air model has the most oxygen dissociation. The large difference between the translational and vibrational temperatures of the thermochemical nonequilibrium gas model indicates that the flow is also in thermal nonequilibrium. Thus, in comparison to cases 1 and 2, this flow exhibits the effects of both nonequilibrium and wall cooling on boundary layer stability.

The corresponding nondimensional spatial amplification rates and phase velocities are shown in Fig. 13. The chemical nonequilibrium

air model yields the most-unstable second-mode disturbances, whereas, in comparison with the chemical nonequilibrium flow, the thermochemical nonequilibrium air model shows that thermal nonequilibrium has a stabilizing effect. However, there is less than a 7% difference in the maximum spatial amplification rates of the three gas models. This suggests that the effects of the thermal and chemical nonequilibrium in air are dominated by the effects of wall cooling. A similar observation was made by Stuckert and Reed[3] in their study of air in chemical nonequilibrium flowing at Mach 25 over a cold wall cone. These observations may also provide clarification of the transition measurements conducted by Germain et al.[17] on a sharp cone in air at high enthalpy. They observed no significant effect on transition Reynolds number because of varying degrees of chemical nonequilibrium.

VI. Conclusions

A computational study of the effects of thermochemical nonequilibrium on the stability of a hypersonic boundary layer has been conducted. The linear, spatial growth of first- and second-mode disturbances in the chemically reacting flow was computed. Three reacting gas models were considered: equilibrium air, chemical nonequilibrium air, and thermochemical nonequilibrium air. Thermal and chemical equilibrium were simulated by adjusting the vibrational relaxation times and chemical reaction rates in the governing equations. This approach to simulating the chemically reacting flow was validated by comparisons to previous results in the literature for perfect gas, equilibrium air, and chemical nonequilibrium airflows.

For the most unstable oblique first-mode disturbances, the thermochemical nonequilibrium air model was found to be more destabilizing than the chemical nonequilibrium air model. In contrast, the equilibrium air model was found to be the least destabilizing compared to both nonequilibrium air models. For the second-mode disturbances, the maximum spatial amplification rates indicated that chemical nonequilibrium was slightly destabilizing, and thermochemical nonequilibrium was slightly stabilizing. For the conditions examined, the results of the second-mode disturbances in equilibrium flow did not differ greatly from the chemical nonequilibrium flow. Furthermore, for these flow conditions, the effect of wall cooling dominated the effects of the different air models. The first-mode disturbances were stabilized because of wall cooling, and the second-mode disturbances were destabilized.

For both adiabatic and cold wall conditions, the second-mode disturbances were found to be the most dominant. Their observed stability behavior clarified two observations in recent high-enthalpy hypersonic flow transition experiments. First, the transition Reynolds number decreased with wall cooling. Whereas this was previously known for hypersonic perfect gas flows, this is newly demonstrated for flows in thermochemical nonequilibrium. Second, for the cases examined, there was no significant effect on transition Reynolds number because of the chemical nonequilibrium of air. Thus, the stability analysis developed in the present work shows promise for development of future hypersonic flight vehicles.

Acknowledgments

Support for this work was provided by NASA under Grant NAGW-1331 to the Mars Mission Research Center at North Carolina State University. The first author received support from Sandia National Laboratories, Albuquerque, New Mexico. Allocation grants from the North Carolina Supercomputing Center and the Minnesota Supercomputer Institute at the University of Minnesota provided time on a Cray Y-MP and Cray C-90, respectively.

References

[1]Malik, M. R., and Anderson, E. C., "Real Gas Effects on Hypersonic Boundary-Layer Stability," *Physics of Fluids A*, Vol. 3, No. 5, 1991, pp. 803–821.

[2]Malik, M. R., "Transition in Hypersonic Boundary Layers," *Fourth Symposium on Numerical and Physical Aspects of Aerodynamic Flows* (California State Univ., Long Beach, CA), 1989.

[3]Stuckert, G., and Reed, H. L., "Linear Disturbances in Hypersonic, Chemically Reacting Shock Layers," *AIAA Journal*, Vol. 32, No. 7, 1994, pp. 1384–1393.

[4]Stuckert, G. K., "Linear Stability Theory of Hypersonic, Chemically Reacting Viscous Flow," Ph.D. Thesis, Dept. of Mechanical and Aerospace Engineering, Arizona State Univ., Tempe, AZ, Dec. 1991.

[5]Lees, L., and Lin, C. C., "Investigation of the Stability of the Laminar Boundary Layer in a Compressible Flow," NACA TN 1115, 1946.

[6]Hudson, M. L., Chokani, N., and Candler, G. V., "Nonequilibrium Effects on Hypersonic Boundary Layers and Inviscid Stability," AIAA Paper 94-0825, Jan. 1994.

[7]Mack, L. M., "Boundary-Layer Linear Stability Theory," *Special Course on Stability and Transition of Laminar Flow*, AGARD Rept. 709, June 1984, pp. 3-1–3-81.

[8]Mack, L. M., "Review of Linear Compressible Stability Theory," *Stability of Time Dependent and Spatially Varying Flows*, edited by D. L. Dwoyer and M. Y. Hussaini, Springer–Verlag, New York, 1987, pp. 164–187.

[9]Hudson, M. L., "Linear Stability of Hypersonic Flows in Thermal and Chemical Nonequilibrium," Ph.D. Thesis, Dept. of Mechanical and Aerospace Engineering, North Carolina State Univ., Raleigh, NC, Feb. 1996.

[10]Candler, G. V., and MacCormack, R. W., "The Computation of Hypersonic Ionized Flows in Chemical and Thermal Nonequilibrium," *Journal of Thermophysics and Heat Transfer*, Vol. 5, No. 3, 1991, pp. 266–273.

[11]MacCormack, R. W., and Candler, G. V., "The Solution of the Navier–Stokes Equations Using Gauss–Seidel Line Relaxation," *Computers and Fluids*, Vol. 17, No. 1, 1989, pp. 135–150.

[12]Malik, M. R., "Numerical Methods for Hypersonic Boundary Layer Stability," *Journal of Computational Physics*, Vol. 86, 1990, pp. 376–413.

[13]Khorrami, M. R., and Malik, M. R., "Efficient Computation of Spatial Eigenvalues for Hydrodynamic Stability Analysis," *Journal of Computational Physics*, Vol. 104, 1993, pp. 267–272.

[14]Golub, G. H., and Van Loan, C. F., *Matrix Computations*, 2nd ed., Johns Hopkins Univ. Press, Baltimore, MD, 1989, pp. 394–406.

[15]Chang, C.-L., Malik, M. R., Erlebacher, G., and Hussaini, M. Y., "Compressible Stability of Growing Boundary Layers Using Parabolized Stability Equations," AIAA Paper 91-1636, June 1991.

[16]He, Y., and Morgan, R. G., "Transition of Compressible High Enthalpy Boundary Layer Flow Over a Flat Plate," *Aeronautical Journal*, Vol. 98, No. 972, 1994, pp. 25–34.

[17]Germain, P., Cummings, E., and Hornung, H., "Transition on a Sharp Cone at High Enthalpy," AIAA Paper 93-0343, Jan. 1993.

K. Kailasanath
Associate Editor